Anomalous boundary deformation induced by enclosed active particles*

Wen-De Tian(田文得)[1,2,†], Yan Gu(顾燕)[1], Yong-Kun Guo(郭永坤)[1], and Kang Chen(陈康)[1,2,‡]

[1] *Center for Soft Condensed Matter Physics & Interdisciplinary Research, College of Physics, Optoelectronics and Energy, Soochow University, Suzhou* 215006, *China*

[2] *Kavli Institute for Theoretical Physics China, Chinese Academy of Sciences, Beijing* 100190, *China*

(Received 5 April 2017; revised manuscript received 18 May 2017; published online 20 August 2017)

We simulate a two-dimensional model of a round soft boundary enclosed with self-propelled particles. Persistent motion drives these particles to accumulate near the boundary, thereby dramatically deforming the boundary shape through collisions. Quantitative analyses of the boundary shape and the particle distribution show that there are two typical regimes in the variation of the morphology with the increase of self-propulsion of particles. One is under small forces, characterized by the radially inhomogeneous distribution of particles and the suppression of local fluctuations of the almost round boundary, and the other is under large forces, featured by the angularly inhomogeneous distribution of particles and the global shape deformation of the boundary. These two features are strongly cooperative. We also find different mechanisms in the particle relocation at low and high particle concentrations.

Keywords: self-propelled particles, boundary, active matter, c onfinement

PACS: 05.40.–a, 64.70.pv, 05.40.Jc **DOI:** 10.1088/1674-1056/26/10/100502

1. Introduction

Active matter refers to a variety of systems ranging from, e.g., cytoskeleton of living cells on a microscopic scale to schools of fish on a macroscopic scale.[1] The common feature of these systems is that the constituent units can move actively (self-propelled) by consuming energy. Such a non-thermal motion is the origin of their out-of-equilibrium nature, which leads to very rich intriguing phenomena, e.g., giant fluctuations,[2,3] spontaneous phase separation,[4,5] and pattern formation.[6,7] In addition to the biological active matters, various artificial active systems have been designed and fabricated, which allow the studies of these nonequilibrium phenomena in well-controlled cases.[2,8–11]

A boundary is ubiquitous in both natural and laboratory active systems. Recent efforts[12–21] have been devoted to understanding the distributions and dynamics of active units confined by hard boundaries with various shapes. The boundary can block and rectify the motions of these active units and cause them to accumulate nearby. The accumulation is greatly influenced by the shape or local curvature of the boundary.[15,18] The non-thermal pressure exerted by the active units in turn can drive the immersed objects with asymmetric boundaries to move directionally.[22–25] In the biological world, the living organisms usually operate with soft boundaries, e.g. molecular motors and microtubules confined by cell membrane, pathogens migrating through the extracellular matrix of the host. Therefore, understanding the interplay between active unit and soft boundary is of fundamental importance.[26–28]

In this paper, we address this problem by studying a simple two-dimensional (2D) model, in which self-propelled disks are confined inside a closed deformable boundary, which is mimicked by spring-connected beads. This system is relevant to the cases where active organisms are enclosed by membranes, other biofilms or flexible surfaces such as the liquid-water interface.[29] It can also be realized by confining microscopic self-propelled particles (SPPs) inside a giant vesicle or using elastomer as the boundary for macroscopic SPPs. We find that persistent motion drives the particles to accumulate near the boundary,[12,13] and dramatically deform its shape through collisions. On the one hand, the boundary deforms when the inhomogeneous aggregation of the particles takes place. On the other hand, the trend of particles accumulating at the place of large curvature,[18] reinforces such a deformation. In the present paper, we are concerned with the variations of the size and shape of the soft boundary and its coupling with the distribution of SPPs.

2. Model and simulation methods

We consider a 2D system where N_p self-propelled particles (treated as disks) are enclosed by a soft boundary. Each particle has mass m, and diameter σ. In addition to the thermal Brownian motion at temperature T, each particle is propelled by a force with the amplitude F through its center. The orientation of the force, $\hat{\mu} = (\cos\theta, \sin\theta)$ rotates with time due to fluctuations. The soft boundary is mim-

*Project supported by the National Natural Science Foundation of China (Grant Nos. 21474074, 21674078, 21374073, and 21574096).

†Corresponding author. E-mail: tianwende@suda.edu.cn

‡Corresponding author. E-mail: kangchen@suda.edu.cn

© 2017 Chinese Physical Society and IOP Publishing Ltd

icked by a ring of spring-connected passive beads ($N_b = 1256$) which are set to be identical to the active particles except being passive, i.e., without propelling force on them. All non-bonded interactions between particles and beads are given by the isotropic and purely repulsive Weeks–Chandler–Andersen (WCA) potential,[30] $U_{WCA}(r) = 4\varepsilon\left[(\sigma/r)^{12} - (\sigma/r)^{6}\right] + \varepsilon$ with a cutoff at $r = 2^{1/6}\sigma$, beyond which $U_{WCA} = 0$, ε is the interaction strength. The bonded harmonic potential between boundary beads is $U_b = k(r - r_0)^2$. We set the spring constant $k = 50000\varepsilon/\sigma^2$ and equilibrium bond length $r_0 = 0.25\sigma$ to prevent the active particles from crossing the boundary. In the natural circular shape, the perimeter of the boundary $L_0 = 314\sigma$, the radius $R_0 \approx 50\sigma$ and the enclosed area $S_0 \approx 7850\sigma^2$.

The motions of particles and beads are described by the Langevin equations as follows:

$$m\ddot{\boldsymbol{r}}_i = -\frac{\partial U_i}{\partial \boldsymbol{r}_i} - \gamma\dot{\boldsymbol{r}}_i + F\hat{\boldsymbol{\mu}}_i(t) + \sqrt{2\gamma k_B T}\boldsymbol{\eta}_i(t), \quad (1)$$

$$\dot{\theta}_i = \sqrt{2D_r}\xi_i(t). \quad (2)$$

Equation (1) governs the translational motion. For the boundary beads, $F = 0$, the potential U_i is composed of the non-bonded WCA potentials and bonded harmonic potentials, and only equation (1) is required. In contrast, for the active particles, U_i contains only the non-bonded WCA potentials and equation (2) which depicts the coupled rotational kinetics of the propelling direction is necessary. The translational friction coefficient $\gamma = k_B T/D_0$ with D_0 being the translational diffusion constant. The rotational diffusion rate $D_r = 3D_0/\sigma^2$ when only thermal noise is present. $\eta_i(t)$ and $\xi_i(t)$ are unit-variance Gaussian white noises.

We use the LAMMPS software to perform the simulations.[31] A square box of $200\sigma \times 200\sigma$ with a periodic condition in both x and y directions is adopted. Reduced units are used by setting $m = 1$, $\sigma = 1$, and $k_B T = 1$. $\tau = \sqrt{m\sigma^2/k_B T}$ is the corresponding unit time. We set $\varepsilon = 10$ and $\gamma = 10$, which is large enough so that the motions of particles and beads are effectively overdamped. We treat D_r as an independent parameter because in many cases the rotational noise is athermal.[12,15] To highlight the influence of the particle activity, we set D_r to be a small value of $7.5 \times 10^{-4}\tau^{-1}$, inverse of which quantifies the persistence time of the active motion. For each case, it runs in a minimum time of $1 \times 10^7\tau$ in time steps of $\Delta t = 0.0025\tau$.

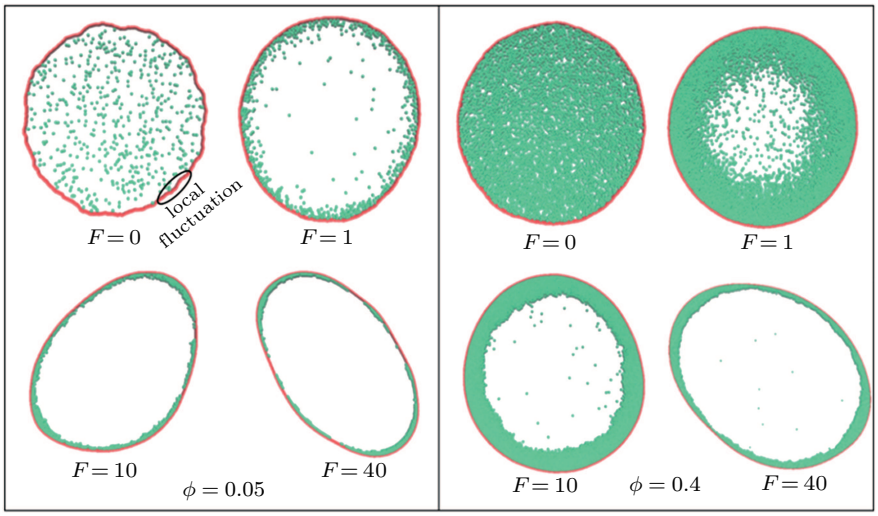


Fig. 1. (color online) Snapshots of the morphologies for the initial particle area fraction $\phi = 0.05$ (left) and 0.4 (right) and varying propelling forces. The red lines represent a soft bead-spring boundary and the green spheres denote active particles.

3. Results

We consider three initial area fractions of confined SPPs, $\phi = 0.05$ (low), 0.2 (medium), and 0.4 (high), where $\phi \equiv \pi\sigma^2 N_p/4S_0$. Figure 1 shows the variations of the typical instantaneous morphologies with the increase of the propelling force on the particles for $\phi = 0.05$ and 0.4. Apparently, in both cases, there are two regimes in the variation of the morphology with increasing propelling force. i) For small propelling force, the distribution of particles inside the closed boundary changes from homogeneous distribution to radially inhomogeneous aggregation, i.e., a concentration hole gradually forms in the center due to enhanced aggregation of particles near the boundary; the shape of the boundary roughly keeps circular; and apparently the local fluctuation of the boundary is increasingly suppressed. ii) For large active force, the distribution of particles becomes both radially and angularly inhomogeneous; the boundary is gradually elongated and deviates from a circle; this global shape deformation is the consequence of the inhomogeneous distribution of the particles along the boundary and the trend of their accumulating around the places of high curvature,[18] which forms positive feedback in the deformation of the boundary. In the following, we quantitatively analyze the variations of the size and shape of the boundary, the inhomogeneous distribution of particles, and their correlations.

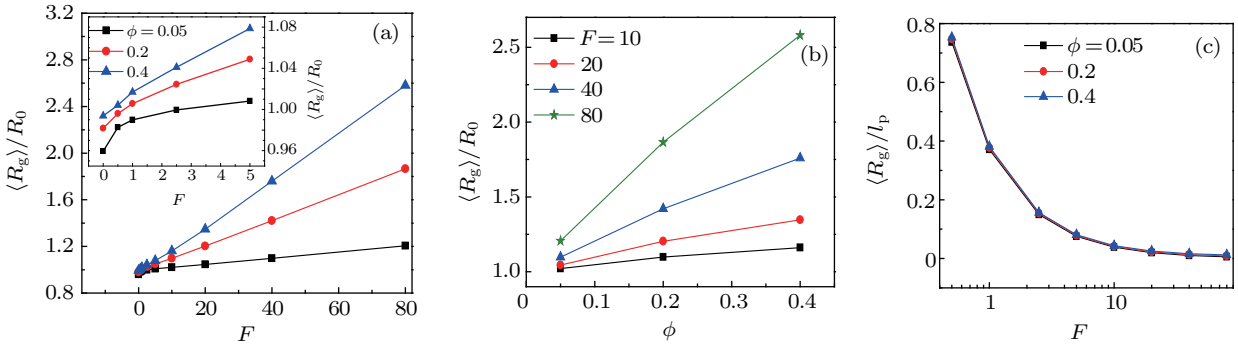


Fig. 2. (color online) Variations of dimensionless mean radius of gyration of the soft boundary with (a) propelling force and (b) the initial particle area fraction, where R_0 is the natural radius of the boundary. The inset in panel (a) shows the magnified parts of curves to show the data at small forces. (c) Linear–log plot of the ratio of the mean radius of gyration of the boundary to the persistence length of a free active particle, $\langle R_g \rangle / l_p$ versus propelling force which quantifies the degree of confinement.

First, we calculate the mean radius of gyration, $\langle R_g \rangle$, of the boundary, based on the positions of its constituent beads, as a measure of its size for a ring polymer (Fig. 2(a)). In two dimensions, the radius of gyration is defined as $R_g \equiv \sqrt{\lambda_L^2 + \lambda_S^2}$, where λ_L and λ_S are the two eigenvalues of the gyration tensor,

$$\Re_{\alpha\beta} \equiv \frac{1}{N_b}\left[\sum_{i=1}^{N_b}\left(r_\alpha^i - r_\alpha^{com}\right)\left(r_\beta^i - r_\beta^{com}\right)\right]\alpha, \quad \beta = x, y, \quad (3)$$

where r_α^i is the α Cartesian coordinate of the i-th bead on the boundary and r_α^{com} is the corresponding center-of-mass coordinate. At large driving forces ($F \geq 10$), good linear relationships are found between $\langle R_g \rangle$ and F for all the three initial area fractions of particles that we have calculated. The slope is larger for higher ϕ. Figure 2(b) shows the variations of $\langle R_g \rangle$ with ϕ under several (large) forces. The curves only slightly deviate from linearity. These nearly linear behaviors can be explained by the following simple scaling argument. Ignoring the noise for translational motion in Eq. (1), the persistence length of a free active particle $l_p = F/\gamma D_r$. The ratio $\langle R_g \rangle / l_p$can, to some extent, account for the degree of confinement.[18] Figure 2(c) shows a dramatic decrease of the ratio at a small force, implying a steep transition from weak to strong confinement with the increase of force. The strong confinement causes the formation of the concentration hole in the center, i.e., the bulk particle density approaches zero (Fig. 1).[18] At a large driving force, the thermal forces are negligible and it corresponds to the situation of strong confinement,[12,18] i.e., all the active particles aggregate near the boundary and exert a force F on it. Therefore, the total force, $F_{expansion}$, exerted by the particles on the boundary, which causes its expansion, is proportional to the strength of the driving force and the number of confined particles. Ignoring the influences of inhomogeneous distribution of particles and the non-circular shape of the boundary, we have roughly, $F_{expansion} \propto \phi F$. This force is balanced by the tension of the boundary, i.e., $F_{expansion} \propto F_{tension} \propto k\pi\left(\Delta R_g\right)/N_b$. Therefore, we have $\Delta R_g \propto \phi F$, i.e., R_g is a linear function of F or ϕ.

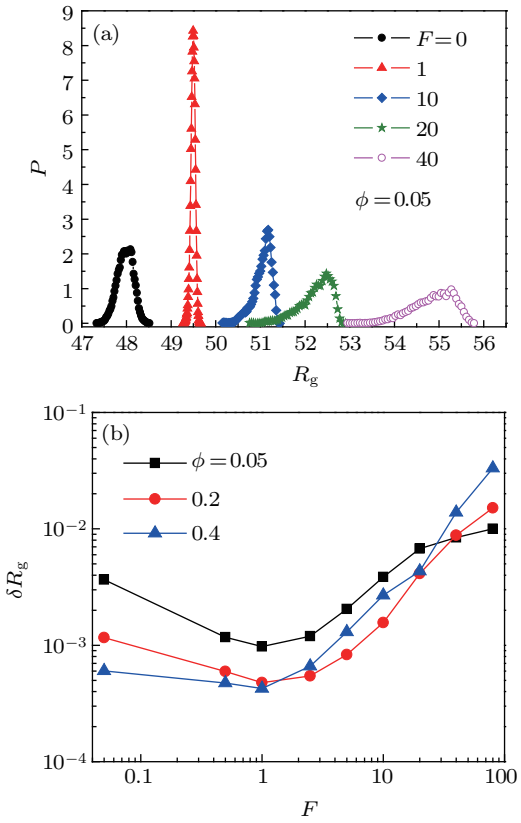


Fig. 3. (color online) (a) Probability distributions of the radius of gyration at various forces for $\phi = 0.05$, and (b) variations of relative fluctuations of the radius of gyration $\delta R_g \equiv \sqrt{\left(\langle R_g^2 \rangle - \langle R_g \rangle^2\right)/\langle R_g \rangle^2}$ with propelling force.

At small F (inset of Fig. 2(a)), we find a crossover from rapid to slow expansion of the boundary with the propelling force around $F = 1$. The initial rapid expansion is attributed to the aggregation of particles to the boundary, which effectively increases the average number of particles that exert a force on the boundary. We calculate the probability distributions of R_g for $\phi = 0.05$ under different forces (Fig. 3(a)). The curve of $F = 1$ shows the narrowest distribution indicating the strong suppression of the local fluctuation of the boundary. This is further proved by the calculation of the relative fluctuation,

$$\delta R_g \equiv \sqrt{\left(\langle R_g^2 \rangle - \langle R_g \rangle^2\right)/\langle R_g \rangle^2}$$

in Fig. 3(b) where minimum fluctuations for all particle area fractions are around $F = 1$. The probability distribution at $F \leq 1$ is left-right symmetric. In contrast, the distribution at large force is asymmetric. These are the manifestations of the characteristics of the two regimes: radial expansion and suppression of local fluctuation of the boundary in regime one and the global shape deformation in regime two.

To quantify the global shape deformation of the boundary, we calculate the asphericity (deviation from a circle)[32,33] in Fig. 4. The asphericity in two dimensions is defined as

$$A = (\lambda_L - \lambda_S)^2/(\lambda_L + \lambda_S)^2, \tag{4}$$

where A is 0 if the shape is circular or isotropic. Figure 4(a) shows that $\langle A \rangle$ increases dramatically when $F > 1$ in the case of $\phi = 0.05$, while a slow-to-rapid increase is found for $\phi = 0.2$ and 0.4. This manifests the different manner (sharp transition at low ϕ versus gradual transition at high ϕ) in the crossover from regime one to regime two with the increase of propelling force. At low ϕ, SPPs form a thin and sparse layer around the boundary at the end of regime one. Upon further increase of the propelling force, the SPPs easily slide along the boundary, which leads to a significant angular anisotropic distribution of particles and hence the shape deformation of the boundary. Therefore, the transition from regime one to regime two at low particle concentration is sharp. Presumably, the crossover happens around the condition satisfying the strong confinement, i.e., $l_p = F/\gamma D_r > 2R_g \Rightarrow F > 0.75$ which is consistent with the observed transition point $F \approx 1$. In contrast, at high ϕ, SPPs form a thick layer around the boundary and enhance the homogeneity of the angular distribution of particles. Consequently, in a large range of propelling force, the particles could not individually slide significantly but collectively along the boundary. Hence, the shape deformation keeps small even though the SPPs are strongly confined. Note that $\langle A \rangle$ for $\phi = 0.05$ shows a clear transition from the rapid to slow increase at a force around $F = 20$. Examining the trajectories, we find the aggregation layer of particles along the boundary becomes thin and sparse for $\phi = 0.05$ and $F \geq 20$ (Fig. 1), and there is no appreciable adjustment of the thickness of the particle aggregation layers along the boundary upon the further increase of the force, which, otherwise, would contribute to the increase of $\langle A \rangle$. Therefore, the slow increase at $F \geq 20$ is induced by the further expansion of the boundary without the contribution or enhancement from the further inhomogeneous angular distribution of active particles.

Time correlation function of asphericity $C(A,t) \equiv \langle (A(t) - \langle A \rangle)(A(0) - \langle A \rangle) \rangle / \langle \Delta A^2 \rangle$ is a way to quantify the varying rate of the global shape (Figs. 4(b) and 4(c)). We find that the force-dependence of the decay is different for the low and high initial particle concentrations. For $\phi = 0.05$, the $C(A,t)$ decays faster (i.e., the shape varies faster) at a larger force (Fig. 4(b)). The change of the decaying rate is appreciable. Taking the time at which $C(A,t) = 0.3$ as the characteristic correlation time, we have that the correlation time changes from $t_c = 505$ for $F = 5$ to $t_c = 218$ for $F = 80$. On the contrary, the decay of $C(A,t)$ becomes slower upon the increase of force for $\phi = 0.4$ (Fig. 4(c)), but apparently the change is small. The correlation time changes from $t_c = 312$ for $F = 5$ to $t_c = 418$ for $F = 80$. There are two competing factors in determining the rate of the shape variation: expansion of the boundary and the activity of the particles, both of which are enhanced with the increase of active force. The large size of the boundary slows down the shape variation while the large activity of particles leads to the rapid relocation and hence the fast shape variation. The expansion of the boundary with active force is weak for $\phi = 0.05$ (Fig. 2(a)) and the enhanced activity of particles dominates and leads to faster decay of $C(A,t)$ at a larger driving force. In contrast, the expansion of the boundary is significant for $\phi = 0.4$ and causes a much slower variation of the shape at a larger force. Notice that the correlation time for

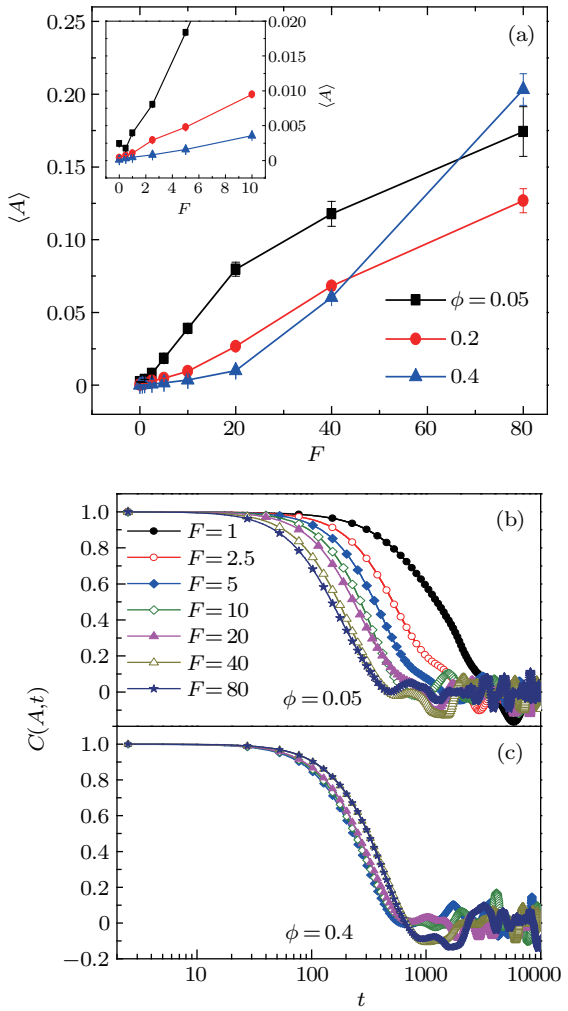


Fig. 4. (color online) (a) Variations of mean asphericity of the boundary with active force; the inset shows the data at small forces. The decay of the time correlation function of asphericity for concentrations $\phi = 0.05$ (b) and 0.4 (c).

$\phi = 0.05$ is larger than that for $\phi = 0.4$ when $F \leq 40$. We examine the trajectories and find that the possible reason is the different mechanisms for the particle relocation. For $\phi = 0.05$ the layer of particles at the boundary is thin and the particles are relocated mostly through the motion along the boundary, while the layer of particles at the boundary is thick for $\phi = 0.4$ and besides the motion along the boundary many particles near the center move across the central hole, which can definitely speed up the change of the angular distribution of particles.

To investigate the radial and angular inhomogeneous distributions of the enclosed particles and their coupling with the deformation of the boundary, we calculate the Gini coefficients[12] G_{r} and

$$G_{\mathrm{a}} = \frac{1}{2N^2\bar{\rho}} \sum_i \sum_j |\rho_i - \rho_j|$$

by partitioning the space in radial and angular directions, respectively (see the inset of Fig. 5(a)), where $\bar{\rho}$ is the mean density, ρ_i the number density of particles in the i-th partitioned space, and N the total number of partitioned spaces. For the radial Gini coefficient, G_{r}, we choose the average position of the boundary beads as the center and divide the center-to-bead lines equally to form inner concentric boundaries which partition the space radially ($N = 40$). We use the angular Gini coefficient, G_{a}, to capture the inhomogeneous distribution of the particles along the boundary. To this end, we choose $N = 40$ beads on the boundary with an interval of around 30 beads and draw circles with the chosen beads as the centers; the radius is empirically set to be $r_{\mathrm{c}} = 0.9L/N$, where L is the perimeter of the boundary. We also try other choices of N and r_{c}, which only quantitatively changes the results. Figure 5(a) shows that for all initial area fractions, G_{r} increases significantly when the force $F \leq 1$ and then gradually approaches a plateau. The turning point from regime one to regime two is around $F \approx 1$ or 2, above which most of the particles aggregate near the boundary. This is in regime one. Below the turning point, we find the angular Gini coefficient G_{a} decreases (Fig. 5(b)). We ascribe this decrease to the suppression of fluctuations of both the particles and the boundary when particles aggregate near the boundary. At a large F, all values of G_{a} increase with force, manifesting the enhanced angular inhomogeneous distribution of particles, which corresponds to the regime two. The crossovers from regime one to regime two are found to be different at low and high values of ϕ. For $\phi = 0.05 G_{\mathrm{a}}$ increases immediately when $F > 1$, i.e., the crossover is sharp. In contrast, G_{a} keeps small and does not rise appreciably until $F > 5$ for $\phi = 0.2$ and $F > 10$ for $\phi = 0.4$, i.e., the crossover is gradual. These behaviors are in consistent with the variations of asphericity in Fig. 4, manifesting a strong correlation between the shape deformation of the boundary and the inhomogeneous angular distribution of particles.

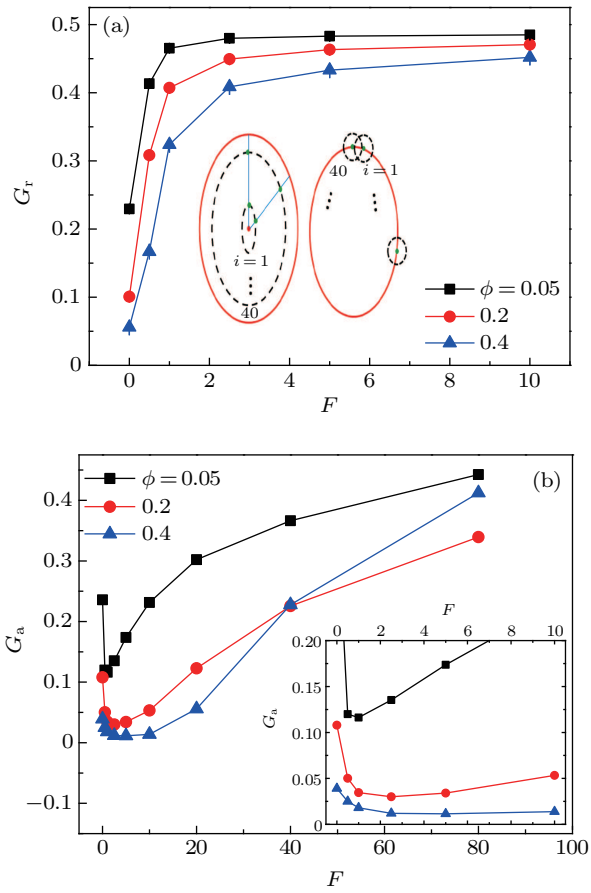


Fig. 5. (color online) (a) Variations of radial Gini coefficient, G_{r}, with propelling force. The inset shows the schematic diagram of partitioning the space radially (left) and angularly along the boundary (right) for calculating the radial and angular Gini coefficients, respectively. (b) Variations of angular Gini coefficient, G_{a}, with propelling force. The inset shows the magnified parts of curves at small forces. (The standard deviations of the data in panels (a) and (b) are less than 0.09 and the standard errors of the mean are less than 4×10^{-4}.)

Finally, we calculate the local curvature κ of the boundary and also the local pressure on it by statistics. The local curvature $\kappa = |y''|/\left(1 + y'^2\right)^{3/2}$, where (x, y) is the coordinate of a boundary point, and y'' and y' are the second and first derivatives with respect to x. The local curvatures are calculated at the bead positions along the boundary in the discrete form of the derivatives. The local pressure exerted by active particles is evaluated by the local force along the local normal direction $\hat{n}$ of the boundary divided by the local arc length. The statistical data for $\phi = 0.05$ are shown in Fig. 6(a). It is found that the local pressure is almost independent of the local curvature at small forces ($F \leq 5.0$), which corresponds to the small asphericity of the boundary as a whole (Fig. 4(a)). For $F \geq 10$, local pressure increases with the increase of the local curvature, which accords with the observation on fixed boundary.[15,18] The correlation between local pressure and local curvature is directly visualized in Fig. 6(b), which shows

the heat map of the local pressure and curvature along the contour of the boundary for the case of $F = 80$ and $\phi = 0.05$.

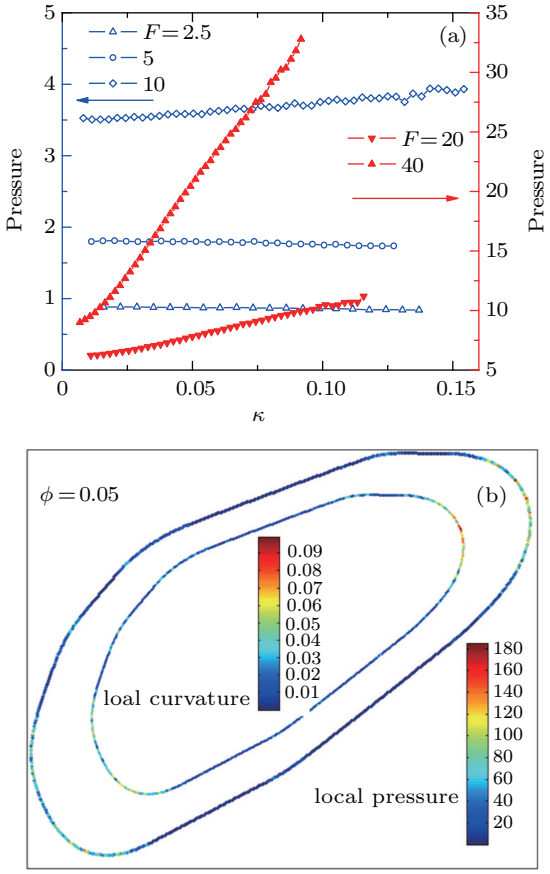


Fig. 6. (color online) (a) Variations of average pressure with local curvature κ for $\phi = 0.05$. (b) Profile of the instantaneous (i.e., the data are extracted from a typical snapshot) local curvature (inside loop) and local pressure (outside loop) along the boundary for the case of $F = 80$, $\phi = 0.05$.

4. Discussion and conclusions

Boundaries are ubiquitous in both natural and laboratory active systems. Understanding the interplay between active agent and boundary is important for both basic science and applications. Although the living organisms usually operate with soft boundaries, the properties of active agents confined by flexible boundaries have been less addressed. In this paper, we study a very simplified 2D model of SPPs confined by a ring-polymer-like boundary. The cooperative phenomenon between boundary fluctuation/shape deformation and particle distribution/collective motion is found. In summary we find that i) the average size of the boundary varies roughly linearly with the propelling force and the number of enclosed particles; ii) there are two typical regimes in the variation of the morphology with propelling force; iii) there is strong coupling between the shape deformation of the boundary and the particle inhomogeneous distribution; iv) the crossover from regime one to regime two is abrupt for small ϕ but is gradual for large ϕ. The mechanism is similar to the case studied by Nikola *et al.*, who found that the pressure inhomogeneity causes a modulation instability of a short semi-flexible filament.[34]

Our model is easily realizable in a granular experiment. Also, in a biological experiment, it shows that colloidal particles can be confined inside a fibroblast cell through phagocytosis which suggests a possible way of realizing our model in a biological system.[35] As a kind of active colloidal cell,[36] this integrated system has the potential to perform some functions as a machine. Our results provide some insights into the control of the shape by, for example, the amplitude of propelling force and particle concentration, which may help design and manipulate the colloidal machine. Moreover, our model captures some essential features of a biological cell: active motion and deformability. It will be interesting to explore the emergent properties of the assembly of these active colloidal cells.

The very first version of this work was uploaded to the arXiv.org in 2015 and cited by the work,[37] in which the authors studied the shape and displacement fluctuations of a soft vesicle filled with anisotropic Run-and-Tumble particles.

References

[1] Marchetti M C, Joanny J F, Ramaswamy S, Liverpool T B, Prost J, Rao M and Simha R A 2013 *Rev. Mod. Phys.* **85** 1143
[2] Deseigne J, Dauchot O and Chaté H 2010 *Phys. Rev. Lett.* **105** 098001
[3] Narayan V, Ramaswamy S and Menon N 2007 *Science* **317** 105
[4] Tailleur J and Cates M E 2008 *Phys. Rev. Lett.* **100** 218103
[5] Cates M E 2012 *Rep. Prog. Phys.* **75** 042601
[6] Cates M E, Marenduzzo D, Pagonabarraga I and Tailleur J 2010 *Proc. Natl. Acad. Sci.* **107** 11715
[7] Surrey T, Nédélec F, Leibler S and Karsenti E 2001 *Science* **292** 1167
[8] Palacci J, Sacanna S, Steinberg A P, Pine D J and Chaikin P M 2013 *Science* **339** 936
[9] Golestanian R 2009 *Phys. Rev. Lett.* **102** 188305
[10] Paxton W F, Kistler K C, Olmeda C C, Sen A, St. Angelo S K, Cao Y, Mallouk T E, Lammert P E and Crespi V H 2004 *J. Am. Chem. Soc.* **126** 13424
[11] Wang W, Duan W, Ahmed S, Mallouk T E and Sen A 2013 *Nano Today* **8** 531
[12] Yang X, Manning M L and Marchetti M C 2014 *Soft Matter* **10** 6477
[13] Chiu Fan L 2013 *New J. Phys.* **15** 055007
[14] Guidobaldi A, Jeyaram Y, Berdakin I, Moshchalkov V V, Condat C A, Marconi V I, Giojalas L and Silhanek A V 2014 *Phys. Rev. E* **89** 032720
[15] Fily Y, Baskaran A and Hagan M F 2015 *Phys. Rev. E* **91** 012125
[16] Chepizhko O and Peruani F 2013 *Phys. Rev. Lett.* **111** 160604
[17] Locatelli E, Baldovin F, Orlandini E and Pierno M 2015 *Phys. Rev. E* **91** 022109
[18] Fily Y, Baskaran A and Hagan M F 2014 *Soft Matter* **10** 5609
[19] Guidobaldi H A, Jeyaram Y, Condat C A, Oviedo M, Berdakin I, Moshchalkov V V, Giojalas L C, Silhanek A V and Marconi V I 2015 *Biomicrofluidics* **9** 024122
[20] Ezhilan B, Alonso-Matilla R and Saintillan D 2015 *J. Fluid Mech.* **781** R4
[21] Jens E and Gerhard G 2015 *Europhys. Lett.* **109** 58003
[22] Angelani L, Di Leonardo R and Ruocco G 2009 *Phys. Rev. Lett.* **102** 048104
[23] He L and Zhang H P 2013 *Europhys. Lett.* **102** 50007

[24] Di Leonardo R, Angelani L, Dell'Arciprete D, Ruocco G, Iebba V, Schippa S, Conte M P, Mecarini F, De Angelis F and Di Fabrizio E 2010 *Proc. Natl. Acad. Sci.* **107** 9541
[25] Sokolov A, Apodaca M M, Grzybowski B A and Aranson I S 2010 *Proc. Natl. Acad. Sci.* **107** 969
[26] Ledesma-Aguilar R and Yeomans J M 2013 *Phys. Rev. Lett.* **111** 138101
[27] Kaiser A and Löwen H 2014 *J. Chem. Phys.* **141** 044903
[28] Zhu L, Lauga E and Brandt L 2013 *J. Fluid Mech.* **726** 285
[29] Pitt W G, McBride M O, Barton A J and Sagers R D 1993 *Biomaterials* **14** 605
[30] Weeks J D, Chandler D and Andersen H C 1971 *J. Chem. Phys.* **54** 5237
[31] Plimpton S 1995 *J. Comput.Phys.* **117** 1
[32] Rudnick J and Gaspari G 1986 *J. Phys. A: Math. Gen.* **19** L191
[33] Harder J, Valeriani C and Cacciuto A 2014 *Phys. Rev. E* **90** 062312
[34] Spellings M, Engel M, Klotsa D, Sabrina S, Drews A M, Nguyen N, Bishop K and Glotzer S C 2015 *Proc. Natl. Acad. Sci. USA (PNAS)* **112** E4642
[35] Kodali V K, *et al.* 2007 *Soft Matter* **3** 337
[36] Nikola N, Solon A P, Kafri Y, Kardar M, Tailleur J, and Voituriе R 2016 *Phys. Rev. Lett.* **117** 098001
[37] Paoluzzi M, Di Leonardo R, Marchetti M C and Angelani L 2016 *Sci. Rep.* **6** 34146